Buoyant convection from a discrete source in closed and leaky porous media

M. R. Flynn[†], Mark A. Roes[†], Chunendra K. Sahu[†] and Diogo Bolster[♣]

[†] Dept. of Mechanical Engineering, Univ. of Alberta (mrflynn@ualberta.ca)
[♣] Dept. of Civil & Environmental Engineering & Earth Sciences, Univ. of Notre Dame

Abstract

By adapting the well-established "filling box" methodology, which describes turbulent convection from a discrete hot or cold spot within a closed or ventilated geometry, we present a new, experimentally-validated model corresponding to laminar plumes rising or falling in a control volume filled with porous media. Model predictions are corroborated by focusing attention on the terminal height of the interface that separates discharged plume fluid from uncontaminated ambient fluid in a ventilated geometry characterized by discrete fissures along the bottom boundary. Two complementary analyses are presented: one that considers a solute dispersion coefficient that is uniform, the other in which this dispersion varies in space. Key similarities and differences with classical filling box models are briefly discussed as are geophysical examples to which this work may be applied.

Keywords: Filling box model; plume; porous media flow; buoyant convection

1 Introduction

Filling box models describe the evolution of a turbulent plume and its outflow within a closed or ventilated control volume. These models trace their origins to the seminal paper by Baines and Turner (1969), who coupled the classical plume theory of Morton et al. (1956) with an equation describing, for a negatively-buoyant plume, the upwards advection of plume fluid that is discharged along the bottom boundary. Some fraction of this discharge is subsequently entrained back into the plume, as a result of which the ambient stratification evolves in a nontrivial fashion. Among many other examples, filling box models have been successfully applied in describing the natural ventilation of the built environment (Linden et al. (1990); Nabi and Flynn (2013)) and flows in chemical storage tanks (Germeles (1975)), but the adaption of this methodology to porous media flow has received little attention. Although the geometries associated with flow in geological strata may be irregular, here too one finds numerous instances of (laminar) thermal or compositional plumes in control volumes that are either closed or ventilated. Examples include the injection of supercritical CO_2 into saline aquifers for purposes of geological sequestration (Bickle (2009)), the dissolution of non-aqueous phase liquids into groundwater (National-Research-Council (2012)) and contaminant leakage from surface waste piles (Kuo and Ritchie (1999)).

The present contribution provides a theoretical and experimental investigation of porous media filling box flows. With reference to recently published work, we shall demonstrate that such models are both straightforward to derive and informative in that they provide experimentally-validated estimates of key parameters of physical interest e.g. for ventilated filling boxes having a dense plume, the terminal height of the interface that separates discharged plume fluid below from uncontaminated ambient fluid above.

Our exposition is organized as follows: in section 2, we outline our theoretical model. Complementary laboratory experiments are described in section 3 and a comparison be-

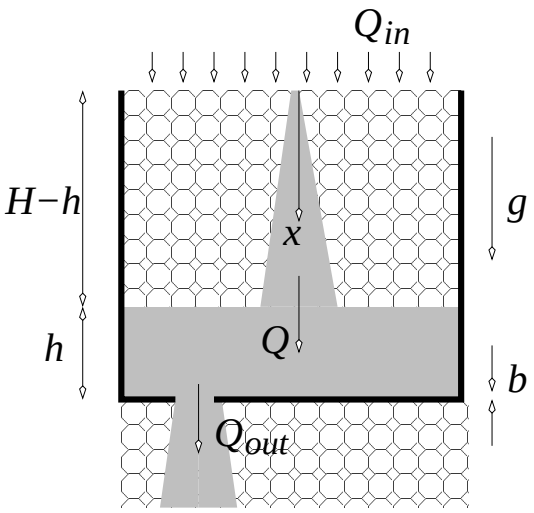

Figure 1: Schematic representation of the rectilinear porous media filling box flow under investigation. The control volume indicated by the thick solid lines extends a distance Λ into the page.

tween theory and measurement in presented in 4. Finally section 5 presents a series of conclusions for the work as a whole.

2 Theory

For simplicity, we consider miscible, Boussinesq fluids and an idealized rectilinear geometry as shown in figure 1 that includes a negatively-buoyant plume source in the middle of the (open) upper boundary. As the plume falls, it entrains external ambient fluid and thereby simultaneously grows in size and decreases in density. Upon reaching the bottom boundary, plume fluid is discharged in the form of oppositely-directed horizontal gravity currents. After these gravity currents reach the lateral sidewalls of the tank, there forms a layer of contaminated fluid that progressively deepens with time, t. The case of an impermeable bottom boundary has been carefully examined by Sahu and Flynn (2015, 2016); most of our present focus concerns a ventilated box containing along this bottom boundary one or more fissures of total cross-sectional area A and permeability k_f. After a long time, the depth, h, of the contaminated layer is constant as is the layer density, ρ_c, which is also spatially uniform. The volumetric rate of outflow through the fissures, Q_{out}, is given as

$$Q_{out} = \frac{Ak_f g'}{\nu}\left(\frac{h+b}{b}\right), \qquad \text{where} \qquad g' = g\left(\frac{\rho_c - \rho_0}{\rho_0}\right). \tag{1}$$

Here ν is the kinematic viscosity and H and b are defined in figure 1 (Neufeld et al. (2009)). Moreover, g is gravitational acceleration and ρ_0 is the density of the uncontaminated layer. In the $t \to \infty$ limit, the density of the contaminated layer equals the plume density at the level of the interface, $x = H - h$. Similarly, Q_{out} must match the plume volume flux at the interface, $Q|_{H-h}$. If dispersion, the process of pore-scale solute transport, can be approximated as spatially-uniform,[1] $Q|_{H-h}$ can be recovered by from the classical analysis of Wooding (1963) whereby

$$Q|_{H-h} = \left[\frac{36D\phi F_0 k(H-h+x_0)\Lambda^2}{\nu}\right]^{1/3}, \tag{2}$$

[1]The case of nonuniform dispersion is considered in the Appendix.

in which D is the dispersion coefficient, F_0 is the plume source buoyancy flux, ϕ and k are, respectively, the porosity and permeability of the medium, Λ is the depth of the line source/control volume and the virtual origin correction, x_0, is defined as

$$x_0 = \frac{Q_0^3 \nu}{36 D \phi F_0 k \Lambda^2}\,, \tag{3}$$

in which Q_0 is the source volume flux. Meanwhile, the plume density, averaged over the plume cross-sectional area, can be determined from the following expression for the area-averaged reduced gravity:

$$\bar{g'}|_{H-h} = \left[\frac{F_0^2 \nu}{36 D \phi k (H - h + x_0)\Lambda^2}\right]^{1/3}. \tag{4}$$

By combining the equations of the last paragraph, it can be shown that $\xi \equiv h/H$, the non-dimensional interface height measured from the bottom boundary, satisfies a cubic polynomial of the form

$$\begin{aligned} 0 &= \left(\frac{A}{\Lambda b}\right)^3 \left(\frac{k_f}{k}\right)^3 \xi^3 + \left[\frac{3b}{H}\left(\frac{A}{\Lambda b}\right)^3 \left(\frac{k_f}{k}\right)^3 - \frac{1}{\mathrm{Ra}}\right] \xi^2 \\ &+ \left[3\left(\frac{b}{H}\right)^2 \left(\frac{A}{\Lambda b}\right)^3 \left(\frac{k_f}{k}\right)^3 + \frac{2}{\mathrm{Ra}}\left(1 + \frac{x_0}{H}\right)\right] \xi \\ &+ \left(\frac{b}{H}\right)^3 \left(\frac{A}{\Lambda b}\right)^3 \left(\frac{k_f}{k}\right)^3 - \frac{1}{\mathrm{Ra}}\left(1 + \frac{x_0}{H}\right)^2. \end{aligned} \tag{5}$$

where the Rayleigh number, Ra ($\gg 1$), is given by

$$\mathrm{Ra} = \frac{F_0 k H}{(36 D \phi)^2 \Lambda \nu} \tag{6}$$

For later reference, the dispersion coefficient, D, that appears in (6) is supposed to solve

$$D^{2/3} = \frac{d}{H}\left(\frac{9\phi F_0 k}{2\Lambda\nu}\right)^{1/3} \left[\left(H + \frac{Q_0^3 \nu}{36 D \phi F_0 k \Lambda^2}\right)^{1/3} - \left(\frac{Q_0^3 \nu}{36 D \phi F_0 k \Lambda^2}\right)^{1/3}\right]. \tag{7}$$

Implicit in (7) is the assumption that D is determined by the product of the porous medium bead diameter and a characteristic speed, here selected as the depth-averaged, far field value for the horizontal entrainment velocity (Freeze and Cherry (1979); Roes et al. (2014)).

Representative solutions of (5) are presented in figure 2, which shows ξ vs. $A/(\Lambda b)$ and Ra for various k_f/k, b/H and x_0/H. As expected ξ increases with increasing source volume flux and with decreasing fissure area, A, or permeability, k_f. Figure 2 gives the impression that ξ likewise increases with decreasing F_0; however, as we shall see below, the effect of the source buoyancy flux on ξ is actually weak because of the factors of F_0 that appear in (7).

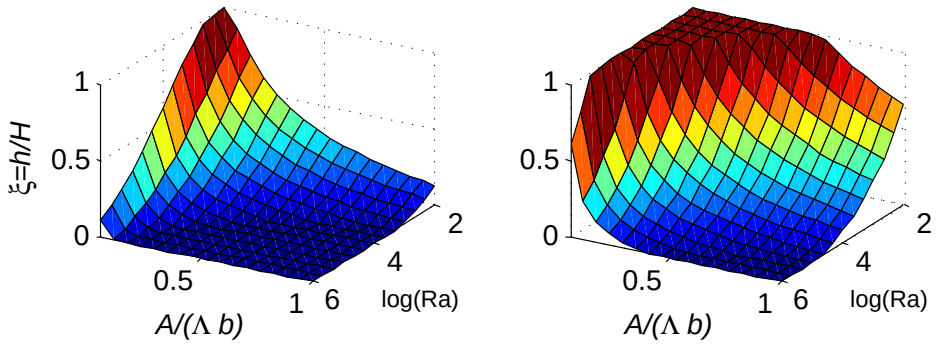

Figure 2: Non-dimensional interface height $\xi = h/H$ as determined from (5). (left) $k_f/k = 1$, $b/H = 0.1$ and $x_0/H = 0.25$. (right) $k_f/k = 0.5$, $b/H = 0.1$ and $x_0/H = 2.0$.

3 Experiments

So as to validate the predictions of the above model, similitude laboratory experiments were run at ambient pressure. Only a brief description of these experiments will be provided here; much more detailed information is available in Roes et al. (2014).

Experiments were run in an acrylic tank measuring 7.6 cm × 32.5 cm × 40.6 cm that was filled to a depth of ∼33.5 cm with 3 mm glass beads. The acrylic tank was, in turn, submerged in 2200 L reservoir that was filled to capacity with tap water. Outflows and inflows from/to the acrylic tank occurred, respectively, through a series of openings located along the bottom boundary and at the top of the front/back sides of the tank. Consistent with the previous discussion, the area available for outflow was much smaller than that available for inflow.

A line source nozzle that spanned the interior tank width was located ∼1.5 cm inside the layer of water-wet beads. It was fed by an overhead tank of large cross section that contained salt water mixed, for purposes of flow visualization, with dye. The plume source volume flux was typically 0.1 mL/s and the source density measured $\rho_s = 1.0114\,\mathrm{g/cm^3}$, $1.0402\,\mathrm{g/cm^3}$ or $1.0700\,\mathrm{g/cm^3}$. Experiments began by opening the flow control valve upstream of the nozzle after which time images were collected at regular intervals using a digital SLR camera. These images were later post-processed to determine, among other parameters, the interface height, which reached its terminal elevation within about 45 min.

For calibration purposes, the "ventilated filling box" experiments described above were supplemented by a series of "emptying box" experiments, which consisted of filling the tank to a predetermined depth with dyed salty fluid of uniform density. The fissures along the bottom boundary were then opened and the time rate of decrease of the lower layer depth was measured. From these experiments, we found that, as with the discharge coefficient that describes flow through an orifice, k_f depends on the density of the draining fluid (see figure 7 of Roes et al. (2014) and Holford and Hunt (2001)).

4 Results

A comparison between theory and experiment is presented in figure 3, which shows, for the three different plume source densities of section 3, experimental measurements of ξ superposed with analogue theoretical predictions. The qualitative agreement is mixed: the data sets indicated by the solid, open and starred symbols all confirm that the interface

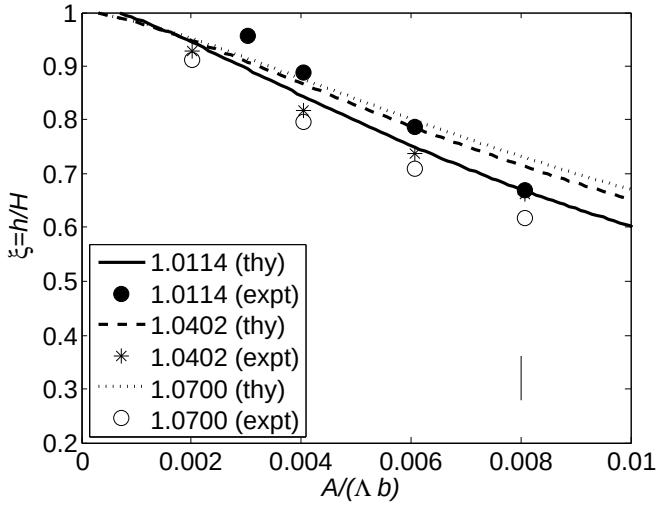

Figure 3: Measured vs. predicted non-dimensional interface height. Caption entries indicate the plume source density in g/cm^3. A representative error for the measured data points is given in the lower right-hand corner.

drops as the area of the fissure(s) increases. On the other hand, our model, in particular (7), leads to the erroneous prediction that, for sufficiently large $A/(\Lambda b)$, the interface increases rather than decreases with increasing ρ_s. The trend of the experimental data is obviously different, however, it is formally surprising that ρ_s does not exert a larger influence, i.e. increasing the source reduced gravity, $\bar{g}'|_0$, by a factor of >5 yields a decrease of ξ of only $\sim$10%. Although the flow physics are different in numerous important respects, this observation nicely complements those of Linden et al. (1990), who made measurements of interface heights in ventilated filling boxes devoid of porous media and containing turbulent plumes. Linden et al. (1990) likewise determined that the interface height is little altered by the plume source density.

Consistent with the above remarks, the quantitative agreement exhibited in figure 3 is encouragingly robust given that no adjustable constants are involved in the derivation of the model equations. More precisely, theory often matches laboratory measurements within experimental error, particularly for small ρ_s.

5 Conclusions

This contribution considers the extension of the filling box flow methodology to porous media buoyant convection of the type exhibited schematically in figure 1. Of particular interest is the terminal elevation of the interface that separates the discharged plume fluid from the uncontaminated ambient. Predictions for this interface height are obtained by matching inflows and outflows to/from the contaminated layer. The salient equation is (5), predictions of which are shown graphically in figures 2 and 3. In the latter case, measured data obtained from similitude laboratory experiments are also included and these show generally favorable agreement with theory.

Equation (5) is derived assuming a spatially uniform solute dispersion coefficient. When this assumption cannot be justified and the the plume centerline velocity is large such that $\mathrm{Pe} \gg \mathcal{O}(1)$ where Pe is the Péclet number, the alternative formulation of appendix A must be applied. As with the classical solution of Wooding (1963), a self-similar plume

solution is again possible. Here, however, it is necessary to divide the solution into inner and outer regions and to introduce a transverse dispersivity that is analogous to the entrainment coefficient used when studying turbulent free plumes.

Acknowledgments
Funding for this research was generously provided by NSERC, Carbon Management Canada and NSF (grant EAR-1113704).

A Nonuniform dispersion

When velocity variations are large so that an average velocity cannot be used in calculating D, one must instead pursue a more detailed theoretical formulation. According to this approach, the governing equations read

$$\frac{\partial u}{\partial x} + \frac{\partial v}{\partial y} = 0 \qquad \text{[mass continuity]}\,, \tag{8}$$

$$\frac{1}{\rho_0}\frac{\partial P}{\partial x} + \frac{\nu}{k}u = \frac{g\rho}{\rho_0} \qquad \text{[momentum cont. in } x\text{]}\,, \tag{9}$$

$$\frac{1}{\rho_0}\frac{\partial P}{\partial y} + \frac{\nu}{k}v = 0 \qquad \text{[momentum cont. in } y\text{]}\,, \tag{10}$$

$$\frac{1}{\phi}\left(u\frac{\partial C}{\partial x} + v\frac{\partial C}{\partial y}\right) \simeq \frac{\partial}{\partial y}\left(D_{\mathrm{T}}\frac{\partial C}{\partial y}\right) \qquad \text{[solute transport]}\,, \tag{11}$$

$$\rho = \rho_0(1+\beta C) \qquad \text{[linear equation of state]}\,. \tag{12}$$

Here u and v are, respectively, the vertical and horizontal components of velocity, P is the fluid pressure, C is the solute concentration, β is the solute contraction coefficient and ρ is the fluid density. Moreover, D_{T} is the (transverse) dispersion coefficient. (Dispersion in the lateral direction is neglected by the boundary layer approximation.)

We consider a flow regime where $\mathrm{Pe} \gg \mathcal{O}(1)$ in which Pe is the Péclet number so that $D_{\mathrm{T}} \simeq \alpha u$ where α is a transverse dispersivity that plays the role of an entrainment coefficient (Houseworth (1984)). Introducing a streamfunction such that $u = \partial\psi/\partial y$ and $v = -\partial\psi/\partial x$, it can then be shown that

$$\frac{\partial^2\psi}{\partial y^2} = \frac{g\beta k}{\nu}\frac{\partial C}{\partial y}\,, \tag{13}$$

$$\frac{\partial\psi}{\partial y}\frac{\partial C}{\partial x} - \frac{\partial\psi}{\partial x}\frac{\partial C}{\partial y} = \alpha\phi\left(\frac{\partial^2\psi}{\partial y^2}\frac{\partial C}{\partial y} + \frac{\partial\psi}{\partial y}\frac{\partial^2 C}{\partial y^2}\right)\,. \tag{14}$$

Sahu and Flynn (2015) demonstrate that (13) and (14) admit self-similar solutions of the form

$$\psi = A_1 x^{1/4}\mathcal{F}(\eta), \quad C = A_2 x^{-1/4}\mathcal{G}(\eta) \tag{15}$$

where $\eta = A_3 y/x^{1/2}$ and the constants A_1, A_2 and A_3 remain to be determined. After some algebra, it can be shown that $\mathcal{G}(\eta) = \mathcal{F}'(\eta)$ provided $A_2 = A_1 A_3 \dfrac{\nu}{g\beta k}$. By extension, and following some further algebraic manipulations, we find that

$$\mathcal{F}'''\mathcal{F}' + \mathcal{F}''\mathcal{F}'' + \frac{1}{4}\mathcal{F}''\mathcal{F} + \frac{1}{4}\mathcal{F}'\mathcal{F}' = (\mathcal{F}''\mathcal{F}')' + \frac{1}{4}(\mathcal{F}'\mathcal{F})' = 0. \tag{16}$$

Of particular interest here is an "inner" (or small η) solution to (16), valid when $\mathrm{Pe} \gg \mathcal{O}(1)$. The "outer" solution corresponds to the region external to the plume; here it is reasonable to ignore spatial variations in the velocity and solute concentration. The division implied by the inner and outer regions is highly reminiscent of "top hat" models of turbulent plumes (Morton et al. (1956)). Upon applying appropriate boundary/symmetry conditions, the following C^0 solutions for $\mathcal{F}$ and $\mathcal{G}$ may obtain:

$$\mathcal{F} = \begin{cases} -c, & \eta < -\pi \\ c \sin \dfrac{\eta}{2}, & -\pi < \eta < \pi \\ c, & \eta > \pi \end{cases} \quad \Rightarrow \quad \mathcal{G} = \mathcal{F}' = \begin{cases} \dfrac{c}{2} \cos \dfrac{\eta}{2}, & -\pi < \eta < \pi \\ 0, & |\eta| > \pi \end{cases} \tag{17}$$

in which c is a constant of integration. After some final simplifications, it can be shown that the plume volume flux is given by

$$Q = \Lambda \int_{-\infty}^{\infty} u \, \mathrm{d}y = \left[\left(\frac{16 F_0 k \Lambda}{\pi \nu} \right)^2 \phi \alpha x \right]^{1/4}, \tag{18}$$

whereas the expression for the plume momentum flux remains the same as in Wooding's case with $\mathrm{Pe} \lesssim \mathcal{O}(1)$, i.e. $M = F_0 k / \nu$.

Two final comments are in order regarding (18). When the plume source is non-ideal ($Q_0 > 0$), we can introduce a virtual origin correction as above so that

$$Q = \left[\left(\frac{16 F_0 k \Lambda}{\pi \nu} \right)^2 \phi \alpha (x + x_0) \right]^{1/4} \qquad \text{where} \qquad x_0 = \frac{1}{\phi \alpha} \left(\frac{\pi \nu}{16 F_0 k \Lambda} \right)^2 {Q_0}^4 . \tag{19}$$

Note moreover that (18) predicts that $Q \sim x^{1/4}$, which is a slower rate of plume growth than the $Q \sim x^{1/3}$ behavior anticipated by (2).

It is straightforward to incorporate (19) into filling box models of either the closed or ventilated type. In the former case, the interested reader is referred to the detailed investigations of Sahu and Flynn (2015, 2016).

References

Baines, W. D. and Turner, J. S. (1969). Turbulent buoyant convection from a source in a confined region. *J. Fluid Mech.*, 37:51–80.

Bickle, M. J. (2009). Geological carbon storage. *Nature Geoscience*, 2:815–818.

Freeze, R. A. and Cherry, J. A. (1979). *Groundwater*. Prentice Hall, Englewood Cliffs, NJ.

Germeles, A. E. (1975). Forced plumes and mixing of liquids in tanks. *J. Fluid Mech.*, 71:601–623.

Holford, J. M. and Hunt, G. R. (2001). The dependence of the discharge coefficient on denity contrast – Experimental measurements. In *Proc. 14th Australian Fluid Mechanics Conf., Adelaide Univ.*, pages 123–126.

Houseworth, J. E. (1984). Longitudinal dispersion in nonuniform isotropic porous media. Technical Report KH-R-45, W. M. Keck Laboratory of Hydraulics and Water Resources, Division of Engineering and Applied Science, California Inst. of Tech.

Kuo, E. Y. and Ritchie, A. I. M. (1999). The impact of convection on the overall oxidation rate in sulfidic waste rock dumps. *Proceedings Mining and the Environment II 1999*, pages 211–220.

Linden, P. F., Lane-Serff, G. F., and Smeed, D. A. (1990). Emptying filling boxes: the fluid mechanics of natural ventilation. *J. Fluid Mech.*, 212:309–335.

Morton, B. R., Taylor, G. I., and Turner, J. S. (1956). Turbulent gravitational convection from maintained and instantaneous sources. *Proc. Roy. Soc. A*, 234:1–23.

Nabi, S. and Flynn, M. R. (2013). The hydraulics of exchange flow between adjacent building zones. *Building and Environment*, 59:76–90.

National-Research-Council (2012). *Alternatives for Managing the Nation's Complex Contaminated Groundwater Sites*. Committee on Future Options for Management in the Nation's Subsurface Remediation Effort and Water Science and Technology Board (WSTB) and Division on Earth and Life Studies (DELS); The National Academies Press.

Neufeld, J. A., Vella, D., and Huppert, H. E. (2009). The effect of a fissure on storage in a porous medium. *J. Fluid Mech.*, 639:239–259.

Roes, M. A., Bolster, D. T., and Flynn, M. R. (2014). Buoyant convection from a discrete source in a leaky porous medium. *J. Fluid Mech.*, 755:204–229.

Sahu, C. and Flynn, M. R. (2015). Filling box flows in porous media. *J. Fluid Mech.*, 782:455–478.

Sahu, C. and Flynn, M. R. (2016). Filling box flows in an axisymmetric porous medium. *Transp. Porous Med.*, 112:619–635.

Wooding, R. A. (1963). Convection in a saturated porous medium at large Rayleigh number or Péclét number. *J. Fluid Mech.*, 15:527–544.